Metrol. Meas. Syst., Vol. XIX (2012), No. 2, pp. 381-394.

PAN POLSKA AKADEMIA NAUK

METROLOGY AND MEASUREMENT SYSTEMS

Index 330930, ISSN 0860-8229

www.metrology.pg.gda.pl

M&MS

USING A SEGMENTED VOLTAGE SWEEP MODE AND A GAUSSIAN CURVE FITTING METHOD TO IMPROVE HEAVY METAL MEASUREMENT SYSTEM PERFORMANCE

José Miguel Dias Pereira[1, 2)], Octavian Postolache[1, 2)], Pedro Silva Girão[2)]

1) Escola Superior de Tecnologia de Setúbal (LabIM), Instituto Politécnico de Setúbal, Rua do Vale de Chaves, Estefanilha, 2910-761 Setúbal, Portugal, (✉dias.pereira@estsetubal.ips.pt, +351 65 790000)
2) Instituto de Telecomunicações, Av. Rovisco Pais, 1049-001, Lisboa, Portugal, (opostolache@lx.it.pt, psgirao@ist.utl.pt, +351.21.8417289)

Abstract

This paper presents a voltammetric segmented voltage sweep mode that can be used to identify and measure heavy metals' concentrations. The proposed sweep mode covers a set of voltage ranges that are centered around the redox potentials of the metals that are under analysis. The heavy metal measurement system can take advantage of the historical database of measurements to identify the metals with higher concentrations in a given geographical area, and perform a segmented sweep around predefined voltage ranges or, alternatively, the system can perform a fast linear voltage sweep to identify the voltammetric current peaks and then perform a segmented voltage sweep around the set of voltages that are associated with the voltammetric current peaks. The paper also includes the presentation of two auto-calibration modes that can be used to improve system's reliability and proposes the usage of a Gaussian curve fitting of voltammetric data to identify heavy metals and to evaluate their concentrations. Several simulation and experimental results, that validate the theoretical expectations, are also presented in the paper.

Keywords: heavy metals measurement, electrochemical analysis, voltammetry, auto-calibration and curve fitting.

1. Introduction

Historically, the voltammetry was developed from the holographic [1, 2] chemical method. This method was discovered by Jaroslav Heyrovsky in the beginning of the 1920s. During the end of the 1950s, the importance of voltammetric methods decreased as they were replaced by spectroscopic methods [3, 4]. After the 1970s, with the advent of low cost and accurate electronic components, namely operational amplifiers, the importance of voltammetric methods became strongly improved because the price of the instruments based on this measuring method got cheaper and their metrological characteristics improved substantially [5-8]. The working principle of voltammetry measurement methods (MM) is based on current measurements when a voltage sweep is applied between two electrodes, namely, the reference electrode (RE) and the working electrode (WE) placed in a cell filled with a water sample. The main advantages of this MM include its large dynamic range, its capability to differentiate between different chemical forms, its high sensitivity, and its suitability to easy integration in automated measuring systems and, above all, its capability to measure several heavy metals (HM) in a single measurement cycle. Beyond the high sensitivity and selectivity of the differential pulse voltammetry (DPV) method, this MM almost cancels measurement errors caused by capacitive effects, namely, double layer effects [1, 9-12] that always exist between the electrodes and the electrolyte. This advantage results from the alternating nature of the voltages used in DPV, particularly in square wave voltammetry (SWV), where the contribution of the electrical current caused by the capacitive double layer effect is negligible,

Article history: received on Nov. 2, 2011; received in revised form on Apr. 24, 2012; accepted on Apr. 30, 2012; available online on May 18, 2012.

as long as the current measurement is performed at a suitable time after the voltage pulse occurrence [1].

This paper is organized in five sections. Section 1 includes papers' introduction. Section 2 presents the measurement principle and the measurement system description, namely its hardware and software parts. Section 3 is dedicated to calibration issues, namely, measurement circuits' and measurement system calibrations, Section 4 that includes several simulation and experimental results. Finally, Section 5 includes paper's conclusions.

2. Measurement System

This section is divided in four parts. It includes a brief description of the measurement principle, the description of the hardware and software parts of the measurement system, and the description of the voltage sweep modes that are used for voltammetry measurements.

2.1. Measurement principle

Fig. 1 represents the three electrodes of a voltammetric cell [13-15], namely, working electrode (WE), counter electrode (CE) and reference electrode (RE). The measurement procedure can be divided in two steps. In the first step, the metals present in the solution are electrochemically reduced in the working electrode (WE) by applying a DC voltage between RE and WE. Then, in the second step, a variable linear voltage or a square wave voltage superimposed to a linear voltage variation are applied between RE and WE, and the current between CW and WE is measured during the voltammetric. After removing voltammogram base line that contains information about the metals residuals in the initial solution (before adding metals' electrolyte), the identification and the concentration of each metal are directly related with the amplitude of the voltammetric voltage and the associated current peaks' amplitudes, respectively. It is important to refer that the square wave voltammetry method assures an excellent low limit of metals' detection (some parts per billion, p.p.b.) [13, 16-18].

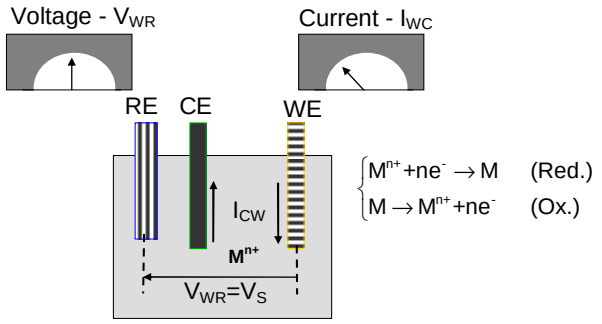

Fig. 1. Three electrodes measuring cell (WE- working electrode; CE- counter electrode; RE- reference electrode; I_{CW}- current between working and counter electrodes; V_{WR}- voltage between working and reference electrodes; V_S- source voltage; Ox.- chemical oxidation equation; Red.- chemical reduction equation; Mn+ dissolved ion).

2.2. Measurement system hardware

Fig. 2 represents the schematic diagram of the electrical circuit that was developed to implement the heavy metal measurement (HMM) system. The circuit includes the following

main elements: a three electrodes measuring cell (MC), a DAQu, and an inverter sum amplifier (OA1), whose input voltage signals come from the DAQu (V_{DAC}) and from the voltage follower circuit (V_{02}). It is important to underline that the linear working condition of OA1 is assured by the negative feedback loop that is closed through the electrolyte solution contained in the MC.

The main characteristics of the A/D converter include a 16 bit conversion resolution, a data acquisition rate equal to 1.25 MS/s and voltage accuracy equal to 52 μV. The main characteristics of the DAC include two 16 bit analog outputs (2.8 MS/s), voltage accuracy equal to 1045 μV and a maximum current drive of the digital outputs equal to 5 mA. These characteristics fulfill all the requirements of the HMM system in terms of accuracy, measurement range, resolution and capability to control several relays [19] that are particularly important for calibration purposes.

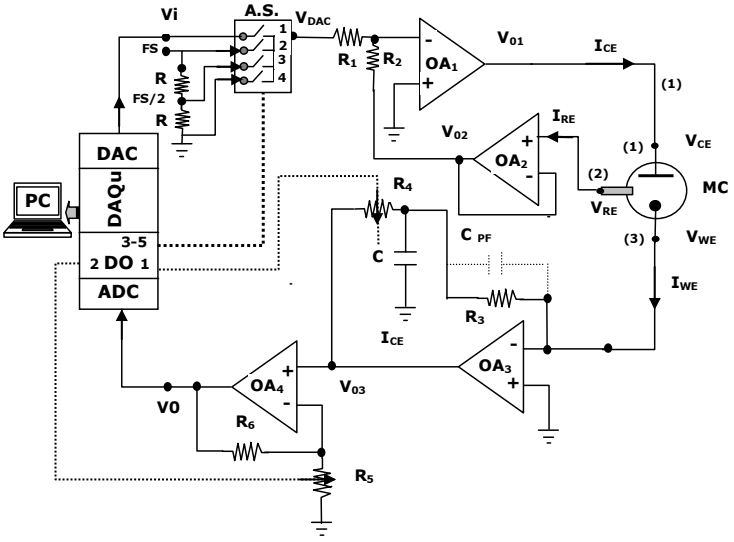

Fig. 2. Schematic diagram of the electrical circuit (MC-measuring cell, DAQu- data acquisition unit, ADC- analog to digital converter, DAC- digital to analog converter, OA- operational amplifier, AS- analog switch).

It must be underlined that the measuring currents are usually very low [20], some tens of nA or even lower, a particular attention must be dedicated to the operational amplifiers characteristics, namely to their input bias and offset currents. Operational amplifiers with input FETs were used because it is essential to obtain an reference electrode current amplitude (I_{RE}) as low as possible relatively to the working electrode current amplitude (I_{WE}). If this condition is not verified, measurements' accuracy is strongly affected because some of the current that comes from the counter electrode (CE) is diverted to the RE and the working electrode current amplitude is lower than the current generated by ions dissolved in the solution. Four LM356 operational amplifiers (OAs) were used to implement the SCu. The main characteristics of these OAs include typical values of bias and offset currents equal to 3 pA and 30 pA, respectively. These current amplitudes assure HMM concentration errors much lower than 1 p.p.b.. Moreover, taking as an example for an I_{CW} current amplitude equal to 100 nA, the relative measurement error caused bias and offset currents is lower than 0.03 % of I_{CW}. Operational amplifiers' voltage offsets are not so critical because they only affect the voltage amplitude that is associated with each voltammetric current peak. These errors are very small and easily compensated by the measuring system's calibration. In what regards the SCu part that is associated with the current to voltage converter (CVC), it is important to

neutralize the effects of the parasitic capacitance (C_{PF}). This requirement is particularly important because the working electrode current (I_{WE}) is very low and the transimpedance gain of the CVC must be, usually, very high. Hence, the parasitic capacitance effects (C_{PF}) must be compensated to minimize current to voltage conversion errors. From the transfer function of the CVC circuit it is possible to conclude that a zero-pole compensation of the CVC circuit can be achieved if the time constants are equal R_4C and R_3C_{PF} [21].
The time constant (R_4C) of the CVC is adjusted by the digital potentiometer R_4 that is controlled through a digital output line of the DAQu. Similarly, digital potentiometer R_5 is used to control the ADC input voltage amplitude according to the ADC full-scale amplitude range.
The MC that was used for testing purposes includes 3 electrodes with the following characteristics: a mercury film milli-electrode (2 mm), used as a working electrode [22], a platinum milli-electrode, used as counting electrode, and a glassy carbone milli-electrode, used as a reference electrode [23].

2.3. Measurement system software

The software of the measurement system was developed with a graphical programming language (LabVIEW). There are several software routines that implement mainly the following tasks: configuration of the measurement system, data acquisition, heavy metals identification and evaluation of their concentrations, auto-calibration, fault detection and data processing.

The software of the measurement system includes a configuration routine that is used to define measurement set-up parameters, namely: electrodes' cleaning time; electro deposition time; wait time; initial voltage scan range; final voltage scan range; voltage step amplitude between adjacent sweep points; square wave pulse duration; current sample mode; pulse amplitude; wait time after each potential jump; segmented voltage sweep ranges; SM (linear, continuous square wave or segmented square wave); selection of heavy metals to measure and the limit of detection (LOD) of the HM concentrations.

The measurement system software also includes a set of routines to implement the Gaussian curve fitting algorithm using a number of Gaussian functions (n) that is equal to the number of current peaks that are contained in the voltammogram. The number of current peaks, obtained from the voltammogram data, are obtained by using a MATLAB function that detects zero-crossings in a smoothed first derivative that exceed a given threshold slope with peaks' amplitudes over a predefined threshold.

Each primary Gaussian function (GFi) is defined by the following relationship:

$$GF_i(V) = k_i \cdot e^{-\frac{(V-\mu_i)^2}{2\sigma_i^2}} \qquad GF(V)=\sum_{i=1}^{n} GF_i(V)\,, \tag{1}$$

where k_i represents the amplitude, μ_i the mean and σ_i the standard deviation of each primary Gaussian function (GF_i).

The Gaussian interpolated curve parameters associated with the mean and amplitude of each primary Gaussian function is used to evaluate heavy metals' redox potentials and associated concentrations, respectively. The standard deviations are also important to evaluate the overlapping degree between Gaussian curves and to validate the interpolation results.

There is a friendly user interface to get voltages and currents from the voltammogram using a set of horizontal and vertical markers. Moreover, there are some software routines that are associated with errors' compensation caused by influencing parameters, particularly, oxygen concentration, temperature and pH whenever the system is integrated in a multi-

parameter WQAS. Fig. 3 represents the front panel of the LabVIEW program. The lower part is used to define measurement configuration parameters and the upper part to display measurement results.

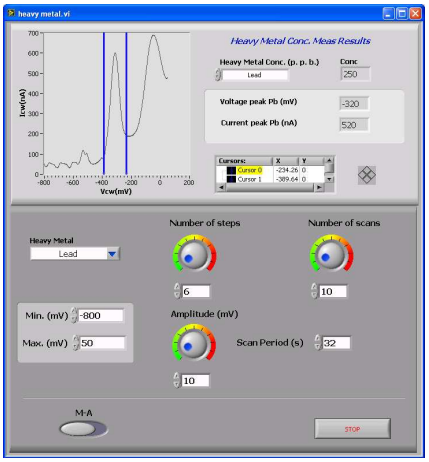

Fig. 3. Front panel of the LabVIEW program.

2.4. Voltage sweep modes

After detecting the current peaks that are associated with dissolved HM with higher concentrations a segmented voltage sweep mode around those current peaks is performed. It can be used two different methods to select the set of voltage ranges that are used for voltammetry purposes. One of this methods requires a previous fast linear SM that identifies the dissolved HM with higher concentrations or, alternatively, a set of predefined voltages, associated with the metals with higher concentration in a given geographical area or associated with the HM that are under assessment, are used. In the first case, the voltage sweep time and resolution of LVS mode are given by [21],

$$T_{LVS} = \frac{(V_{CW})_{max} - (V_{CW})_{min}}{(S.R.)_{LVS}}$$
$$R_{LVS} = \frac{(V_{CW})_{max} - (V_{CW})_{min}}{(\Delta\Delta V_{LVS}} \tag{2}$$

where $(V_{CW})_{max}$ and $(V_{CW})_{min}$ represent the maximum and minimum values of the voltage sweep range, and S.R. and ΔV represent the sweep rate and the voltage increment between adjacent sweep points, respectively. This SM is characterized by a linear and continuous voltage variation (V_{RW}) over time and is used before the final HMM phase. For a typical voltage scan range equal to 1 V and for a sweep rate equal to 0.05 V/s, the T_{LSW} value is equal to 20 s.

In the second case, that is used usually for monitoring purposes, the HM that are under observation are well-known and are obtained from the historical measurement data for a given geographical area. Instead of using a continuous square wave SM, that increment the voltages between $V_{CW})_{max}$ and $(V_{CW})_{min}$, a segmented square wave SM is performed around specific voltage ranges that are associated with the redox potential of the HM under observation. So, a much lower measurement time is achieved, when identical values of the voltage sweep parameters are used, or a much higher measurement resolution and accuracy can be achieved if a slower voltage sweep rate or a lower voltage increment between adjacent sweep points is

used. Obviously there is a compromise between these two advantages, since if a much lower voltage increment between sweep points is used, for the same voltage sweep rate, the measurement time increases. Considering relationship (2), it can be obtained the ratio between segmented square wave (SSW) and continuous square wave (CSW) measurement time durations, T_{SSW} and T_{CSW} that is given by

$$\frac{T_{SSW}}{T_{CSW}} = \frac{\sum_{i=1}^{N} \Delta V_{CWi}}{(V_{CW})_{max} - (V_{CW})_{min}} \cdot \frac{(S.R.)_{CSW}}{(S.R.)_{SSW}}, \quad (3)$$

where $(S.R.)_{SSW}$ and $(S.R.)_{CSW}$ represent the sweep rate for SSW and CSW, respectively, ΔV_{CWi} represents the voltage sweep amplitude around each metal's redox potential under analysis, and $(V_{CW})_{max}$ and $(V_{CW})_{min}$ represent the minimum and maximum values of the sweep voltage range, respectively. From (3) it is possible to conclude that for equal values of sweep rates, a substantially reduction of the HMM measurement time can be obtained if the sum of voltage sweep amplitudes around each metals' redox potential that is under analysis is much lower than the sweep voltage range.

As an example, Fig. 4 represents the HMM time for SSW and CSW SM when the ratio between the sum of voltage sweep amplitudes, around each metal redox potential, and the voltage sweep range is equal to 0.1. The graph was obtained for a sweep rate variation between 0.1 and 10 mV/s, 5 mV voltage increments between adjacent sweep points, and a voltage sweep range equal to 1 Volt.

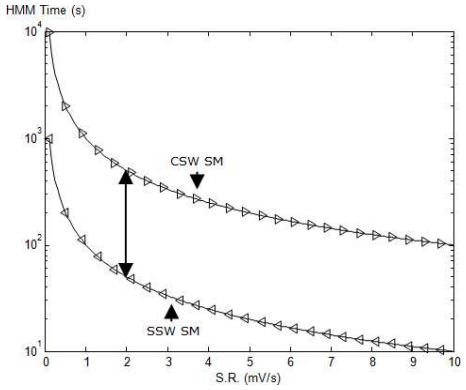

Fig. 4. HMM time for SSW and CSW sweeping modes (ratio between the sum of voltage sweep amplitudes and the voltage sweep range equal to 0.1, ΔV_{CW}=5mV and a sweep voltage range amplitude equal to 1 V).

As it is clearly shown, there is a substantial measuring time reduction associated with SSW SM. For example for a S.R. equal to 2 mV/s the measurement time for SSW and CSW SM are equal to 50 s and 500 ms, respectively. Moreover, it must be underlined that the measuring time ratio, obtained from (3), can be even lower when there is a few numbers of heavy metals under analysis, which is the usual case that is found in WQAS applications.

3. Calibration

Two different auto-calibration modes can be used to improve measurement system reliability. One calibration mode performs the calibration of the HMM circuits and data acquisition devices, excluding the MC, and the second mode performs a complete calibration of the HMM system, including its MC

3.1. Measurement circuit calibration

A dummy cell is used for HMM circuits' auto-calibration purposes. A set of four dip-switches are used to select four different load types, namely, a Randle's [24] circuit (RC_{Cell}), a pure resistive load (R_{Cell}), a pure capacitive load (C_{Cell}), and a parallel association of two signal diodes with opposite forward current directions (D_{Cell}), being each cell type selected by analog switches SW4, SW5, SW6 and SW7, respectively. The analog switch SW3 is used to test the reference sub-circuits of the HMM. Fig. 5 represents the dummy cell and its connection to the potentiostat unit (PT_U).

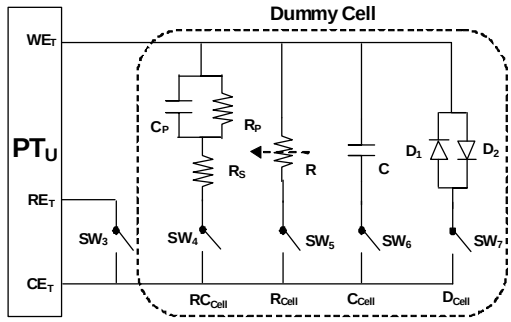

Fig. 5. Dummy cell and its connection to the PT_U (PT_U- potentiostat unit; SW- analog switch; RD_{Cell}- Randle's circuit cell; R_{Cell}- pure resistive cell; C_{Cell}- pure capacitive cell and RD_{Cell}- diode cell).

Different voltage sweep rates, voltage SM, voltage increments between adjacent sweep points and voltage step amplitudes can be used to calibrated the analog and digital parts of the HMM circuits. Regarding the voltage SM, the voltage-to-current characteristic of each cell circuit and its derivative are obtained if a linear SM or a square wave SM are used, respectively [21]. It must be underlined that the Randle's circuit mimics the load presented by a real electrochemical cell. Resistance R_P models the cell polarization resistance, C_P models the interfacial double-layer capacitance and R_S models the solution resistance. Figure 6 represents the voltage-to-current characteristic of the RC_{Cell} for the following set of parameters: R_S=2 MΩ (upper curve), R_S=4 MΩ (lower curve), R_P=20 MΩ and C_P=30 pF. Both tests were performed using a linear voltage SM, a voltage step amplitude equal to 100 mV and a sweep rate equal to 1 mV/s. It can be easily verified that the experimental values of the maximum and minimum current amplitudes and the current time constant, that were experimentally obtained, confirm the theoretical expectations expressed by relationships (4), with a maximum error, relatively to maximum amplitude of the measuring variable, lower that 5%. It is important to underline that this maximum error is, afterwards, compensated using data processing algorithms.

$$I_{\max} = \frac{V_O}{R_S}, \quad I_{\min} = \frac{V_O}{R_S = R_P}, \quad t = C \times \frac{R_S \times R_P}{R_S + R_P}, \tag{4}$$

where I_{max} and I_{min} represent the maximum and minimum RC_{Cell} current amplitudes, respectively, V_0 represents the voltage step amplitude and the time constant (τ) represents the time required for current reducing of 63.2% of initial value (I_{max}).

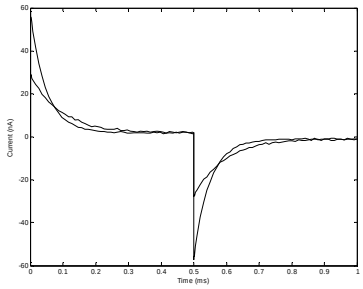

Fig. 6. Voltage-to-current characteristic of the RC_{Cell} for the following set of parameters: R_S=2 MΩ (upper curve), R_S=4 MΩ (lower curve), R_P=20 MΩ and C_P=30 pF.

Regarding signal-to-noise ratio, Fig. 7 represents the histogram of measurement errors when RC_{Cell} is set up with the following set of parameters: R_P=20 MΩ, C_P=30 pF and R_S=2 MΩ. From the measurement data it can be obtained a mean measurement error equal to -0.03 nA, a standard deviation measurement error equal to 0.28 nA and a signal-to-noise ratio almost equal to 41.8 dB.

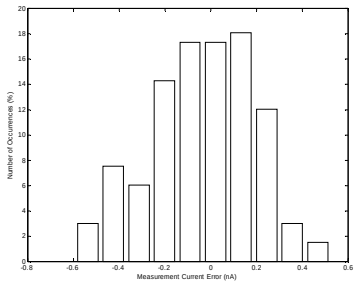

Fig. 7. Histogram of measurement errors when RC_{Cell} is configured with the previous set of parameters, R_P=20 MΩ and C_P=30 pF, and R_S=2 MΩ

3.2. Measurement system calibration

The MSC is based on a set of standard solutions with well-known values of heavy metals concentrations [25]. Fig. 8 represents the calibration diagram that is used for MSC.

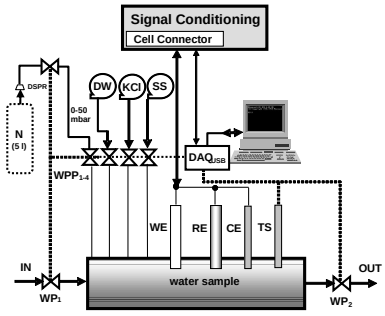

Fig. 8. Measurement system calibration diagram (DAQu- data acquisition unit, DW- deionized water, KCl- potassium chloride, SS- standard solution(s), N- nitrogen gas, WP- water pump, WPP- water peristaltic pump, WE- working electrode, RE- reference electrode, CE- counter electrode, TS- temperature sensor).

The implementation of this calibration mode requires not only a set of standard solutions (SS), but also a nitrogen gas cylinder and two containers, one for deionized water (DW) and another for the support electrolyte, potassium chloride (KCl), in this case. A set of water peristaltic pumps (WPPi) are used to control fluids' flow rate. The number of standard solutions depends on the required measurement accuracy and on the heavy metals that are under measurement. A single standard solution with well-known concentrations of different heavy metals can be used for calibration purposes. The nitrogen gas, contained in a small volume cylinder (5 l), is used to remove oxygen from the solution, being this procedure essential to measure very low concentration levels of heavy metals. Chemical reactions of oxygen contained in water interfere with the measurement of most metal ions. The support electrolyte minimizes solution's ionic activity, reduces to a negligible level the transport of the analytical due to electrostatic field, and assures a minimal value of solution's conductivity. Measurement accuracy is strongly affected by the ionic activity of the metals' ions that are present in the measuring solution. Since the redox potential of each metal also depends on temperature according to the Nernst equation, a temperature sensor (TS) is used to compensate errors caused by temperature variations.

Fig. 9 depicts the measurement apparatus used for calibration purposes.

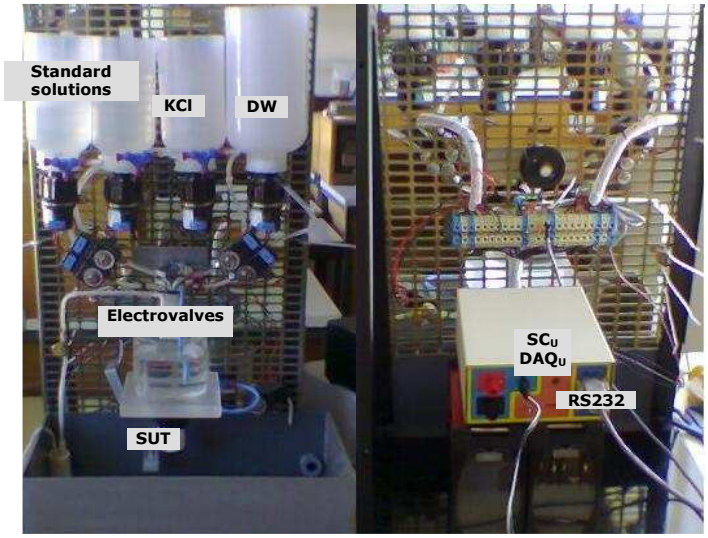

Fig. 9. Measurement apparatus used for calibration purposes (DW- deionized water, SUT- solution under test, SCu- signal conditioning unit, DAQu- data acquisition unit).

4. Results

This section includes several simulation and experimental results. In what regards the simulation results, different curve fitting methods of voltammetric data are tested and the relative performance is evaluated. Measuring system performance is evaluated using the proposed HMM method for a set of water samples taken from a river estuary.

It is important to underline that, in terms of HMM celerity, it is essential to minimize the number of measurement points that are required to obtain a predefined measurement accuracy. If an excessive number of measurement points are used, the computational load for curve fitting purposes is increased and data interpolation errors can be substantially increased due to over fitting [26].

4.1. Simulation Results

There are a large number of methods that can be used for curve fitting of voltammetric data [27-32]. However, some of those methods are unnecessarily complex and there exist little information about the different curve fitting methods' performance. Gaussian curve fitting of voltammetric data is in principle a suitable solution to perform HMM. The mean values of each Gaussian fitting curve are associated with heavy metals' redox potentials and their peaks are associated with heavy metals' concentrations. Figs 10 and 11 represent the Gaussian curve fitting results and associated errors, respectively, for a solution that contains three different heavy metals. The continuous line represents the normalized voltammetric data used for simulation purposes, and the dotted line represents the curve fitting results. Voltage values are normalized against voltage sweep range and current values are normalized against maximum current amplitude.

In this simulation, the curve fitting function is defined by

$$\mathrm{gfit}(x) = \sum_{i=1}^{3} a_i \cdot e^{-((x-b_i)/c_i)^2} \quad . \tag{5.1}$$

The coefficients of the three Gaussian functions that minimize the LMS error, between voltammetric and Gaussian curve fitting data, are given by:

$$\begin{aligned}
&\text{Gaussian coefficients}\\
&\text{(with 95\% confidence bounds):}\\
&a1 = 0.995 \quad (0.9934, 0.9966)\\
&b1 = 0.885 \quad (0.8845, 0.8854)\\
&c1 = 0.113 \quad (0.109, 0.1169)\\
&a2 = 0.887 \quad (0.8848, 0.8894)\\
&b2 = 0.573 \quad (0.5732, 0.574)\\
&c2 = 0.054 \quad (0.05155, 0.05724)\\
&a3 = 0.143 \quad (0.1404, 0.1445)\\
&b3 = 0.326 \quad (0.3239, 0.3288)\\
&c3 = 0.06391 \quad (0.04509, 0.08273)
\end{aligned} \tag{5.2}$$

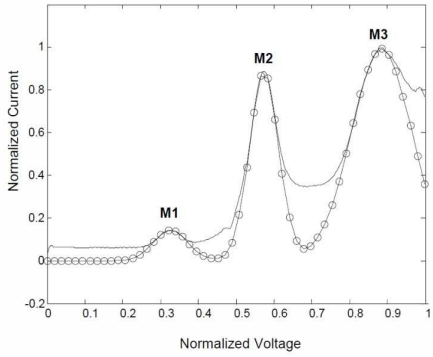

Fig. 10. Gaussian curve fitting results for a solution with three different heavy metals (M1, M2 and M3).

In this case, Fig. 11 shows clearly that the Gaussian curve fitting errors, around voltammogram current peaks, are lower than 1% relatively to measurement data.

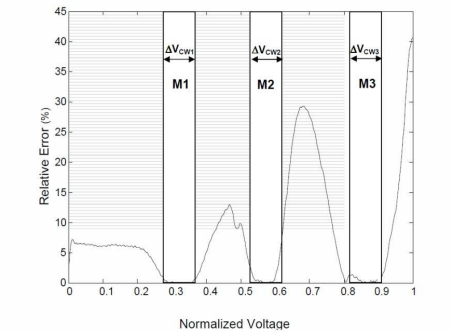

Fig. 11. Gaussian curve fitting errors for a solution with three different metals (M1, M2 and M3).

Additionally, if the Gaussian curve fitting is based on a SSW voltage sweep, around the redox potential of each metal, the curve fitting errors are even lower. However, it is important to refer that if a very narrow voltage sweep interval around the metals' redox potentials is used for curve fitting purposes, the interpolation errors can increase substantially, particularly if the measured data contains outlier measurement values [26].

4.2. Experimental results

A set of three water samples were used for testing purposes. The solutions were collected at the same place of a river estuary but with different tidal conditions, namely, tide levels and tidal current directions and intensities.

Fig. 12 represents the voltammograms obtained for each water sample. Dotted curves are obtained by using a CSW SM for a metals' pre-concentration time of 30 s. The voltage sweep range that was used for voltammetric measurements varies between -800 mV and 50 mV, and the voltage increment between adjacent sweep points is equal to 1 mV. This means that a complete voltage sweep produces 851 measurement points. Using the proposed SSW SM around metals' redox potentials (graph shaded area), the number of measurement points is reduced to 24 and the maximum relative error, around current peaks after Gaussian curve fitting, is lower than 4% relatively to measurement data.

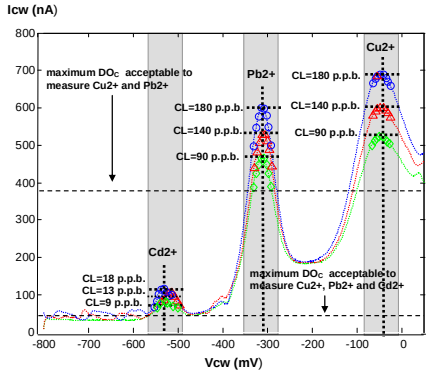

Fig. 12. Voltammograms of the water samples used for testing purposes (dotted line– CSW SM; circles – SSW SM for the low tide condition , triangles - SSW SM for the rising tide condition, diamonds - SSW SM for the high tide condition).

Fig. 13 represents the relative errors of the measurements taking as reference the measurements obtained with a CSW voltage sweep between -800 mV and 50 mV, using the same S.R. and voltage increment between sweep points that were used in the SSW SM.

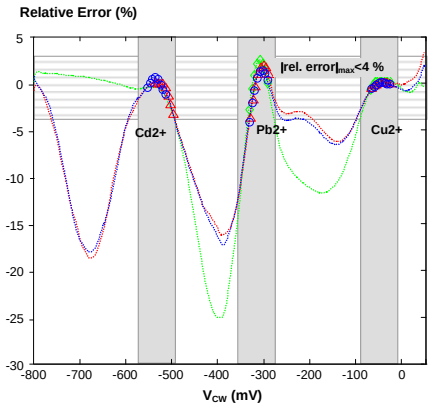

Fig. 13. Relative errors of measurements taking as reference the errors that are obtained when a complete voltage sweep with a voltage increment per sweep point equal to 1 mV (circles - higher concentration level, triangles - medium concentration level, diamonds - lower concentration level).

The experimental results show clearly that each water sample has its own HM concentrations but the main metals that are contained in every sample are the same (Cd, Pb and Cu). It is important to underline that the results that were obtained confirm the ones already obtained by other researchers [33, 34] in the same river estuary by using different HMM methods.

Regarding to measurement time, as long as equal values of CWS and SSW sweep rates and voltage increments between adjacent sweep points are used, there is a substantial reduction of measuring time. For a S.R.=1 mV/s, the measurement time is reduced from 850 s to 24 s, which means a 35 reduction coefficient with a negligible measurement error increment.

5. Conclusion

This paper presents a segmented voltage sweep mode and a Gaussian curve fitting method that can be used successfully for heavy metals measurements based on voltammetry techniques. A particular attention is dedicated to the measurement system accuracy, celerity and reliability that are essential in water quality assessment systems. The measurement system includes two auto-calibration modes. One mode performs the measurement circuit's calibration, excluding the MC, and the other performs a complete calibration of the HMM, including the MC. From the combined results of both calibrations it is possible to identify and diagnose some measurement system faults. Concerning data processing, a Gaussian curve fitting of measurement data is proposed and its performance evaluated. The experimental results that were obtained, for a sample solution with three different heavy metals, show that the number of measurement points can be substantialy reduced with a negligible measurement error increment around voltammetric current peaks.

References

[1] Bard, A.J., Faulkner, L.R. (1980). *Electrochemical Methods*. New York, Wiley.

[2] Sawer, D.T., Sobkowiak, A., Roberts, J.L. (1995). *Electrochemistry for Chemists*. 2nd ed., New York, Wiley.

[3] Rukin, E.M. (2000). Unified Measurements in Determining Traces of Dissolved Metals by Optical Spectroscopy. *Journal Measurement Techniques. Publisher Springer New York*, 43(3), 281-284.

[4] Alexander, D.R., Poulain, D.E., Ahmad, M.U., Kubik, R.D., Cespedes, E.R. (1994). Environmental Monitoring of Soil Contaminated with Heavy Metals using Laser-Induced Breakdown Spectroscopy. In *Geoscience and Remote Sensing Symposium*, 2, 767-769.

[5] Kovaleva, S.V., Gladyshev, V.P., et al. (2005). Methods of Stripping Voltammetry in System of Monitoring Priority Ecotoxicants in Objects of An Environment. In *Proceedings of Korean International Symposium on Science and Technology*, 1, 186-187.

[6] Simion, M., Angelescu, E.E., et al. (2002). Micro and Nanoelectrode Voltammetric Measurements. In *Semiconductor Conference*, 1, 123-126.

[7] Chernyshova, N.N., Svintsova, L.D., Perevezentseva, D.O., Yurasova, S. (2004). Investigation of Electrochemical Activation Phenomenon of Aqueous Medium by Voltammetry Methods, Science and Technology. In *Proceedings. The 8th Russian-Korean International Symposium*, 2, 16-20.

[8] Scozzari, A., Acito, N., Corsini, G. (2005). Signal Analysis of Voltammetric Data Series for Water Quality Tests and Classification. In *Instrumentation and Measurement Technology Conference*, Pisa, Italy, 89-92.

[9] Baudot, A., Bret, J.L. (2003). A Simple Capacitive Cell for the Measurement of Liquids Dielectric Constant Under Transient Thermal Conditions. *CryoLetters*, 24, 5-16.

[10] Mutoh, N., Inoue, T. (2007). A Control Method to Charge Series-Connected Ultraelectric Double-Layer Capacitors Suitable for Photovoltaic Generation Systems Combining MPPT Control Method. *IEEE Trans. on Industrial Electronics*, 54(1), 374-383.

[11] Kaya, A., Fang, H.-Y. (1997). Identification of Contaminated Soils by Dielectric Constant and Electrical Conductivity. *Journal of Environmental Engineering*, 123(2).

[12] Korthum, G. (1965). *Treatise on Electrochemistry*. University of Tubingen, Germany. 2nd ed. by American Elsevier Publishing, New York.

[13] Simion, M., Angelescu, E.E., et al. (2002). Micro and Nanoelectrode Voltammetric Measurements. In *Semiconductor Conference*, 1, 123-126.

[14] Chernyshova, N.N., Svintsova, L.D., Perevezentseva, D.O, Yurasova, S. (2004). Investigation of Electrochemical Activation Phenomenon of Aqueous Medium by Voltammetry Methods, Science and Technology. In *Proceedings. The 8th Russian-Korean International Symposium*, 2, 16-20.

[15] Scozzari, A., Acito, N., Corsini, G. (2005). Signal Analysis of Voltammetric Data Series for Water Quality Tests and Classification. In *Instrumentation and Measurement Technology Conference*, Pisa, Italy, 1, 89-92.

[16] Kovaleva, S.V., Gladyshev, V.P., et al. (2005). Methods of Stripping Voltammetry in System of Monitoring Priority Ecotoxicants in Objects of An Environment. In *Proceedings of Korean International Symposium on Science and Technology*, Korea, 1, 186-187.

[17] Avram, M., Angelescus, A., et al. (2001). Fast Scan Cyclic Voltammetry Simulation for Silicon Nanoelectrodes. In *Semiconductor Confere*nce, Sinaia, Romania, 1, 43-46.

[18] Luther, W.G., Richard, T.D., Theberge, S., Olroyd, A. (1996). Determination of Metal (bi)Sulfide Stability Constants of Mn2+, Fe2+, Co2+, Ni2+, Cu2+, and Zn2+ by Voltammetric Methods, *Environmental Science & Technology*, 30.

[19] Siemens Semiconductor Group, V23100-S0302-A210 Solid State Relays. (October 2009). *http://pdf1.alldatasheet.com/datasheet-pdf/view/133470/SIEMENS/V23100-S0302-A210.html*.

[20] Keithley. (2002). Low Level Measurements – Precision DC Current, Voltage and Resistance Measurements. 5th ed.

[21] Dias Pereira, J.M., Postolache, O., Silva Girão, P. (2010). Improving Celerity of Heavy Metals Measurements. In *IEEE International Instrumentation and Measurement Technology Conference - I2MTC/2010*, Austin, USA, 1, 1073-1077.

[22] Yosypchuk, B., Fojta, M., Barek, J. (2009). Preparation and Properties of Mercury Film Electrodes on Solid Amalgam Surface, Electroanalysis. In *Proceedings of the International Conference on Modern Electroanalytical Methods*, Prague, Czech Republic.

[23] Princeton Applied Research. Micro-Cell Kit K0265 Datasheet: *http://www.princetonappliedresearch.com/Our-Products/Accessories/Micro-Cell-Kit.aspx.*

[24] Franks, W., Schenker, I., Schmutz, P., Hierlemann, A. (2005). Impedance characterization and modeling of electrodes for biomedical applications. In *IEEE Transactions on Biomedical Engineeering*, 52(7), 1295-1302.

[25] Postolache, O., Girão, P., Ramos, H.G., Dias Pereira, M. (2005). Auto Calibration of Stand-Alone Field Operating Sensors for Distributed Water Quality Monitoring Systems. In *14th IMEKO TC4 Symposium on New Technologies in Measurement and Instrumentation, IMEKO TC4*, Gdynia, Poland.

[26] Dias Pereira, J.M., Silva Girão, P., Postolache, O. (2001). Fitting Transducer Characteristics to Measured Data. *IEEE Instrumentation & Measurement Magazine*, 4(4), 26-39.

[27] O'Halloran, R.J., Smith, D.E. (1978). Fast Fourier transform based interpolation of sampled electrochemical data. *Anal. Chem*., 50(9), 1391-1394.

[28] Kano, K., Mori, K., Uno, B., Goto, M. (1990). Voltammetric and Spectroscopi Properties of the Amonia Adduct of Pyrroloquinoline Quinone. *Journal of Electroanalytical Chemistry and Interfacial Electrochemistry*, 293(1), 177-184.

[29] Fleming, B.D., Barlow, N.L., Zhang, J, Bond, A.M., Armstrong, F.A. (2006). Application of power spectra patterns in Fourier transform square wave voltammetry to evaluate electrode kinetics of surface-confined proteins. *Anal Chem*. 1, 78(9), 2948-2956.

[30] Baranski, A., Szulborska, A. (1994). A fourier transform square-wave voltammetry. *Journal of Electroanalytical Chemistry*, 373(1-2), 157-165.

[31] Zheng, X., Mo, J., Cai, P. (1999). Spline wavelet in the resolution of overlapping voltammetric peaks. *Science in China Series B: Chemistry*, Publisher Science China Press, co-published with Springer, 42(2), 145-152.

[32] Huanga, W., Hendersonb, T.L.E., Bondc, A.M., Oldhamd, K.B. (1995). Curve fitting to resolve overlapping voltammetric peaks: model and examples. *Analytica Chimica Acta*, 304(1), 1-15.

[33] Vale, C., Cortesão. Zinc. (2003). Copper and cadmium in the oyster Crassostrea angulata from the Sado estuary. *M. Astruc. and J.N. Lester publication,* Division Heavy metals in the Hydrological cycle, Selper ltd., London, 257-264.

[34] Vale, C., Sandby, B. (1982). A survey of the elemental composition of the bottom sediments in the Sado estuary. In *Proceedings Actual problems of oceanography in Portugal. Ed. JNICT/NATO*, 189-200.